

Lanthanide-Induced Photoluminescence in Lead-Free Cs<sub>2</sub>AgBiBr<sub>6</sub>Bulk Perovskite: Insights from Optical and Theoretical Investigations

*Original*

Lanthanide-Induced Photoluminescence in Lead-Free Cs<sub>2</sub>AgBiBr<sub>6</sub>Bulk Perovskite: Insights from Optical and Theoretical Investigations / Schmitz, F.; Guo, K.; Horn, J.; Sorrentino, R.; Conforto, G.; Lamberti, F.; Brescia, R.; Drago, F.; Prato, M.; He, Z.; Giovanella, U.; Cacialli, F.; Schlettwein, D.; Meggiolaro, D.; Gatti, T.. - In: THE JOURNAL OF PHYSICAL CHEMISTRY LETTERS. - ISSN 1948-7185. - 11:20(2020), pp. 8893-8900. [[10.1021/acs.jpcllett.0c02317](https://doi.org/10.1021/acs.jpcllett.0c02317)]

*Availability:*

This version is available at: 11583/2977501 since: 2023-03-27T14:40:54Z

*Publisher:*

American Chemical Society

*Published*

DOI:[10.1021/acs.jpcllett.0c02317](https://doi.org/10.1021/acs.jpcllett.0c02317)

*Terms of use:*

This article is made available under terms and conditions as specified in the corresponding bibliographic description in the repository

*Publisher copyright*

ACS postprint/Author's Accepted Manuscript

This document is the Accepted Manuscript version of a Published Work that appeared in final form in THE JOURNAL OF PHYSICAL CHEMISTRY LETTERS, copyright © American Chemical Society after peer review and technical editing by the publisher. To access the final edited and published work see <http://dx.doi.org/10.1021/acs.jpcllett.0c02317>.

(Article begins on next page)

# Lanthanide Induced Photoluminescence in Lead-Free Cs<sub>2</sub>AgBiBr<sub>6</sub> Bulk Perovskite: Insights from Optical and Theoretical Investigations

Fabian Schmitz,<sup>1,2</sup> Kunping Guo,<sup>3§</sup> Jonas Horn,<sup>1,4§</sup> Roberto Sorrentino,<sup>5</sup> Gioele Conforto,<sup>2,4</sup> Francesco Lamberti,<sup>6</sup> Rosaria Brescia,<sup>7</sup> Filippo Drago,<sup>8</sup> Mirko Prato,<sup>8</sup> Zhubing He,<sup>9</sup> Umberto Giovanella,<sup>5</sup> Franco Cacialli,<sup>3</sup> Derck Schlettwein,<sup>1,4\*</sup> Daniele Meggiolaro,<sup>10\*</sup> Teresa Gatti<sup>1,2\*</sup>

<sup>1</sup> Center for Materials Research (LaMa), Justus Liebig University, Heinrich Buff Ring 16, 35392 Giessen, Germany

<sup>2</sup> Institute of Physical Chemistry, Justus Liebig University, Heinrich Buff Ring 17, 35392 Giessen, Germany

<sup>3</sup> Department of Physics and Astronomy and London Center for Nanotechnology, University College London, London, WC1E 6BT, United Kingdom

<sup>4</sup> Institute of Applied Physics, Justus Liebig University, Heinrich-Buff-Ring 16, 35392 Giessen, Germany

<sup>5</sup> Istituto CNR di Scienze e Tecnologie Chimiche “Giulio Natta” (CNR-SCITEC), Via Corti 12, 20133 Milano, Italy

<sup>6</sup> Department of Chemical Sciences, University of Padova, via Marzolo 1, 35131 Padova, Italy

<sup>7</sup> Electron Microscopy Facility, Istituto Italiano di Tecnologia (IIT), via Morego 30, 16163 Genova, Italy

<sup>8</sup> Materials Characterization Facility, Istituto Italiano di Tecnologia, via Morego 30, 16163 Genova, Italy

<sup>9</sup> Department of Materials Science and Engineering, Shenzhen Key Laboratory of Full Spectral Solar Electricity Generation (FSSEG), Southern University of Science and Technology, No. 1088, Xueyuan Rd., Shenzhen 518055, Guangdong, China

<sup>10</sup> Computational Laboratory for Hybrid/Organic Photovoltaics (CLHYO), Istituto CNR di Scienze e Tecnologie Chimiche “Giulio Natta” (CNR-SCITEC), Via Elce di Sotto 8, 06123 Perugia, Italy

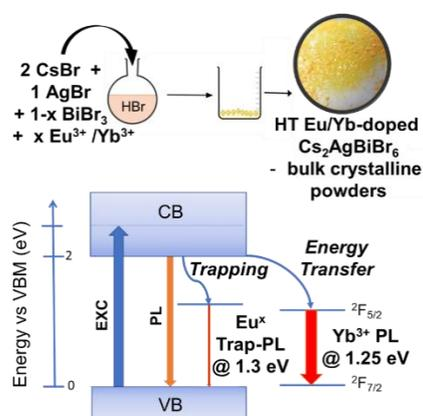
§ These two authors contributed equally

Correspondence to: [teresa.gatti@phys.chemie.uni-giessen.de](mailto:teresa.gatti@phys.chemie.uni-giessen.de); [daniele.meggiolaro@cnr.it](mailto:daniele.meggiolaro@cnr.it); [derck.schlettwein@app.phys.uni-giessen.de](mailto:derck.schlettwein@app.phys.uni-giessen.de)

## Abstract

Emphasis was recently placed on the  $\text{Cs}_2\text{AgBiBr}_6$  double perovskite as a possible candidate to substitute toxic lead in metal halide perovskites. However, its poor light-emissive features currently make it unsuitable for solid-state lighting. Lanthanides doping is an established strategy to implement luminescence in poorly emissive materials, with the additional advantage of fine-tuning the emission wavelength. We discuss here the impact of Eu- and Yb-doping on the optical properties of  $\text{Cs}_2\text{AgBiBr}_6$  thin films, obtained from solution-processing of hydrothermally synthesized bulk crystalline powders, by combining experiments and density functional theory calculations. Eu(III) incorporation does not lead to the characteristic  $^5\text{D}_0 \rightarrow ^7\text{F}_2$  emission feature at 2 eV, while only a weak trap-assisted sub band-gap radiative emission is reported. Oppositely, we demonstrate that incorporated Yb(III) leads to an intense and exclusive photoluminescence emission in the near-infrared as a result of the efficient sensitization of the lanthanide  $^2\text{F}_{5/2} \rightarrow ^2\text{F}_{7/2}$  transition.

## TOC Graphic



The development of lead-free halide perovskites for optoelectronic applications (solar cells, light-emitting diodes –LED-, lasers and photodetectors) is central to current materials research,<sup>1-4</sup> with the aim of finding valuable alternatives to lead-based perovskites, currently leading the field. Lead halide perovskites (LHP) feature a problematic toxicity caused by lead and a limited environmental stability.<sup>5</sup> Double perovskite structures, containing pairs of cations in the +I and +III oxidation states in substitution of  $\text{Pb}^{2+}$  are particularly appealing due to the impressive resistance to ambient stress (humidity, light, heat). Among others, bismuth(III)-based compounds such as  $\text{Cs}_2\text{AgBiBr}_6$  have been the subject of extensive investigations because of the excellent stability and low toxicity.<sup>6-8</sup> The optoelectronic properties of  $\text{Cs}_2\text{AgBiBr}_6$  are, however, strongly limited by the indirect nature of the band-gap, originating by the alternating Ag/Bi-based hexabromide octahedra in the lattice. The existence of a highly localized Bi-based optical transition with pronounced excitonic character and the strong electron-phonon coupling further limit the efficiency of the exciton separation and promote charge recombination in the material, as described in detail by some of us in previous work.<sup>9</sup> These drawbacks, in conjunction with the difficulties in obtaining good-quality thin films,<sup>7,10,11</sup> are the cause of the poor power conversion efficiency (generally below the 3% threshold) achieved up to now by  $\text{Cs}_2\text{AgBiBr}_6$  as the photosensitizer in multi-layered photovoltaic architectures.<sup>12,13</sup> The use of  $\text{Cs}_2\text{AgBiBr}_6$  in LED is also hampered by its poor photoluminescence (PL) properties caused by the non-radiative de-activation of injected electron-hole pairs.<sup>14</sup>

Lanthanide-doping is a well-established strategy to improve luminescence features of wide band-gap inorganic semiconductors<sup>15</sup> and other hybrid solid-state materials,<sup>16</sup> with the possibility of tuning the emission wavelength. As the f-f transitions in lanthanides have normally very low absorption coefficients, crystalline host matrices play the role of sensitizers for boosting efficient emission from these dopants. Lanthanide-doping has been extensively applied also in low band-gap halide perovskites to tune luminescence while maintaining excellent light-absorption and charge transport properties. The success of this structural modification is ensured by the octahedral coordination that characterizes the metal ions in the perovskite lattice.<sup>17,18</sup> In particular, Eu(III) ions and Yb(III) have been employed to tune the PL of LHP nanocrystals in the visible and near-infrared (NIR) ranges, respectively, resulting in materials characterized by very narrow emission peaks typical of the lanthanide-based f-f electronic transitions and high values of the PL quantum yield (PLQY). Quantum cutting processes are associated to Yb-doping in lead halide perovskite nanocrystals,<sup>19</sup> a phenomenon for which PLQY exceeding the ideal value of 100% are measured, thus prospecting application in devices such as NIR-LEDs, with great interest for biomedical applications. Yb-doping has been recently implemented also in lead-free  $\text{Cs}_2\text{AgBiBr}_6$  nanocrystals

by Chen and coworkers, with dopant concentrations of up to 5%.<sup>20</sup> This process has led to the expected tuning of the PL behavior, with introduction of a narrow and intense PL at around 1.25 eV. These studies indicate that the activation of Yb<sup>3+</sup> ions emission is possible also in indirect band gap halide perovskite. The successful sensitization of Yb(III) with the associated NIR emission have been also observed in porous silicon,<sup>21</sup> another indirect band gap semiconductor,<sup>22</sup> highlighting that the indirect nature of the band gap does not affect the emission properties of rare earth do-pants.

Despite their versatility and the generally high PLQY,<sup>23</sup> halide perovskite nanocrystals still find limited use in solid-state applications due to the difficulties in obtaining homogeneous layers employing standard solution processing methods, coupled to the presence of surface defects, which quench PL and trap electrical charges diffusing across the film.<sup>24–26</sup>

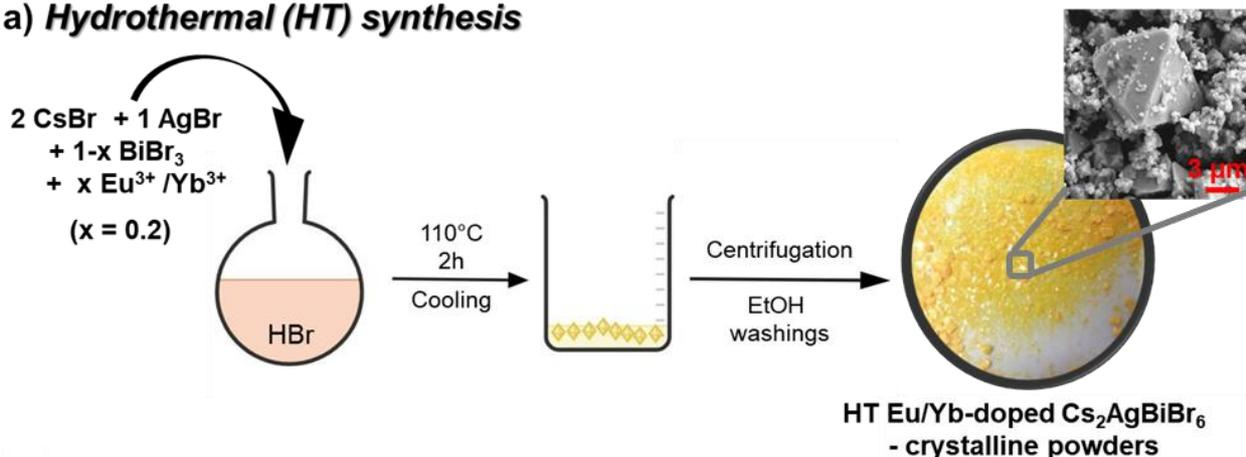
In this work we explore the possibility of doping bulk Cs<sub>2</sub>AgBiBr<sub>6</sub> with lanthanides so as to obtain easy-to-process and homogeneous thin films for light-emitting devices. The impact of Eu- and Yb-doping on the absorption and emission properties of Cs<sub>2</sub>AgBiBr<sub>6</sub> polycrystalline thin films is evaluated through a combined experimental-computational approach. Our analysis shows that both Eu(III) and Yb(III) are incorporated in bulk Cs<sub>2</sub>AgBiBr<sub>6</sub>, and can be photo-excited through the electron transfer from the conduction band (CB) of the host perovskite to mid-gap unoccupied f orbitals. These defects, however, undergo different emissive decay channels. Eu(III) incorporation does not lead to the characteristic <sup>5</sup>D<sub>0</sub>→<sup>7</sup>F<sub>2</sub> emission feature at around 2 eV, but mainly decays through a trap-like recombination mechanism, while Yb(III) shows an intense emission in the NIR, as a result of the efficient sensitization of the lanthanide <sup>2</sup>F<sub>5/2</sub>→<sup>2</sup>F<sub>7/2</sub> transition.

Cs<sub>2</sub>AgBiBr<sub>6</sub> is not normally processed into photoactive thin films by applying the typical protocols used for lead-based perovskites, but requires a previous step of hydrothermal (HT) synthesis to produce its crystalline powder. Once isolated, the product is re-dissolved in a suitable solvent for halide perovskite processing (typically DMSO) and then undergoes the same process employed for the lead-based analogs. Indeed, the simple direct mixing of the metal salts precursors (namely, CsBr, AgBr and BiBr<sub>3</sub>) in DMSO and subsequent processing, do not generally provide phase pure thin films of the Cs<sub>2</sub>AgBiBr<sub>6</sub> double perovskite, as residual peaks of the components or other side-phases (such as the bismuth perovskite Cs<sub>3</sub>Bi<sub>2</sub>Br<sub>9</sub>) are often detected in the X-ray diffraction (XRD) profiles.<sup>27</sup>

The HT process used for the production of Eu(III) and Yb(III) doped Cs<sub>2</sub>AgBiBr<sub>6</sub> is sketched in Fig. 1a (details in the Experimental Section in the Supporting Information - S.I.) and leads to two orange crystalline solids identical to the un-doped Cs<sub>2</sub>AgBiBr<sub>6</sub>, containing crystals with sizes ranging from 500 nm up to 6 μm (see also Fig. S1 for a transmission electron microscopy image),

with the typical octahedral shape of this compound.<sup>12</sup> Employing this synthetic method, we attempted substitution of the  $\text{Bi}^{3+}$  ions in the double perovskite lattice by either  $\text{Eu}^{3+}$  or  $\text{Yb}^{3+}$  up to 20% (the Goldschmidt tolerance factor is not expected to change significantly even at concentrations of these particular dopants up to 50%). In all cases, we could not achieve more than the 0.04% atomic substitution of  $\text{Bi}^{3+}$  with the lanthanides (as determined through elemental analysis, details in the S.I.), pointing out at a very low doping level in the final product.

### a) Hydrothermal (HT) synthesis



### b) Thin films processing

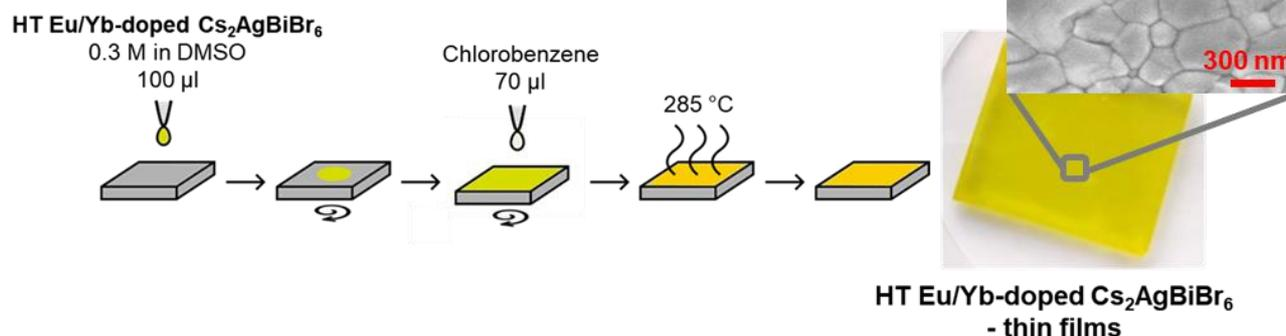


**Figure 1.** Synthesis, characterization and thin film processing of bulk Eu- and Yb-doped Cs<sub>2</sub>AgBiBr<sub>6</sub>. a) Sketch of the hydrothermal synthesis process, with picture and SEM image of a prototypical crystalline product. b) Sketch of the anti-solvent method used for the preparation of thin films, with picture and top-view SEM image of a prototypical film.

Powder XRD of the Eu- and Yb-doped Cs<sub>2</sub>AgBiBr<sub>6</sub> bulk crystalline powder is reported in Fig. S2 of the S.I. indicating preparation of the undoped and doped materials in constant crystal structure, without the presence of any additional compound, but of at least two phases characterized by a higher and lower symmetry. Detailed peak analysis of the (004) reflection at about 31° (most

intense one) was carried out, showing that the signal is constituted of more than one single component (the same accounts for all the other peaks in the XRD powder pattern), due to the presence of at least two phases characterized by different symmetries. The results of this analysis are purely qualitative and are discussed in the S.I.

Bulk doping through the HT method is apparently characterized by a dramatically lower doping efficiency compared to the nanocrystalline form of the material. Differences are likely associated to the dissimilar dimensionality of the host materials, i.e. nanocrystals easily accommodate dopants by forming surface defects, and the employed synthetic techniques. The lower doping in the present case can also be due to the high solubility of the lanthanide precursors we employed in HBr (the medium in which the HT reaction takes place).

For the preparation of thin films, the HT product is dissolved in DMSO and this precursor solution is spin coated, treated with an anti-solvent<sup>28</sup> and finally annealed to improve the crystallization, as depicted in Fig. 1b. The preparation was adapted according to refs.<sup>9,29</sup> and was further optimized with respect to minimized surface roughness, as measured by confocal microscopy. Variation was performed for rotational speed during spin-coating, concentration of the precursor solution, atmosphere during film preparation and choice of the anti-solvent. Best results were obtained by following the procedure described in the experimental methods in the S.I. Dissolved precursor materials in DMSO were investigated as alternative precursor solution for thin film preparation but yielded films of lower quality with smaller crystallites and residues of unreacted precursor materials, leading to additional XRD signals (Fig. S3).

The optimized procedure based on dissolved HT product provides thin films with a thickness of  $82 \pm 5$  nm measured by a profilometer and confirmed by SEM cross sections (Fig. S4), of high quality in terms of grain size (about 280 nm) and absence of pinholes, as analyzed by top-view SEM (inset of Fig. 1b). Phase pure  $\text{Cs}_2\text{AgBiBr}_6$ <sup>27,30</sup> is obtained in the films, pointing either at an effective recrystallization of the material upon reprecipitation and annealing that remove the low symmetry component or at a superposition of the signals within broadened peaks (Fig. S3). Furthermore, in SEM-EDX spectra of the Eu-doped thin film, a very weak signal of Eu was even detected (Fig. S5). To track possible variations of charge distribution within the band structure of the double perovskite following lanthanide doping, the work function (WF) of the thin films was extracted employing Kelvin probe force microscopy (KPFM) (Fig. S6). While the WF value of undoped  $\text{Cs}_2\text{AgBiBr}_6$  is found at 5.07 eV, in agreement with previous reports on  $\text{Cs}_2\text{AgBiBr}_6$  highly crystalline thin films,<sup>10</sup> a 50 meV shift toward smaller values (higher Fermi level) is found for the Eu-doped sample (a small variation is found also for the Yb-doped one, i.e. a small broadening of the overall Gaussian

distribution at the lower energy limit). These findings indicate a slight variation of the Fermi level due to the introduction of defects<sup>31</sup> in the double perovskite structure following lanthanide doping. The presence of defects appears more clearly when examining the UV-visible absorption features of the thin films of the lanthanide-doped compared to undoped Cs<sub>2</sub>AgBiBr<sub>6</sub> reported in Fig. 2a. The three absorption spectra do not differ significantly, except for the indicated (dark grey arrow) increase of the absorbance at low-energy (from 2.7 eV to almost 2.0 eV) in the two doped samples, indicating an increased density of sub-band-gap defect states compared to the undoped semiconductor. As it can be further observed from these spectra, a strong exciton peak centered at 2.83 eV is detected for all the samples, which has been also attributed to a direct s-p electronic transition centered on bismuth<sup>10,32</sup> (real origin still under heated debate<sup>33,34</sup>) and can be seen as a highly localized excitation that does not contribute significantly to the photo-generation of charges in the thin film.<sup>9</sup> The intense (and dominant) Raman mode centered at 177 cm<sup>-1</sup> is strongly related to this excitonic feature and is maintained after doping (Fig. 2b, in full agreement with previous literature data<sup>9,35</sup>).

While the impact of the Eu/Yb-doping in Cs<sub>2</sub>AgBiBr<sub>6</sub> is not significant in the optical properties of the thin films in terms of light absorption (no features ascribable to the direct excitation of lanthanide-based transitions are detected in the spectra in Fig. 2a), significant differences emerge when the emissive behaviors are analyzed. The steady-state PL behavior of the undoped, Eu-doped and Yb-doped thin films of Cs<sub>2</sub>AgBiBr<sub>6</sub> (Fig. 2) has been measured, with a view to detecting specific emission features from lanthanide dopants in the crystal lattice.<sup>17</sup> The PL of pristine Cs<sub>2</sub>AgBiBr<sub>6</sub> consists of the broad/weak emission with large Stokes' shift observed earlier (also indicated as a sign of the strong electron-phonon coupling in this material<sup>14</sup>) centered at around 2 eV (black curve in Fig 2a), which in earlier works was assigned either to emission from self-trapped excitons<sup>9</sup> or to a color center.<sup>14</sup> After doping, the bulk double perovskite with Eu<sup>3+</sup> ions no emissive peaks typical of this lanthanide(III) ion (with the most intense <sup>5</sup>D<sub>0</sub>→<sup>7</sup>F<sub>2</sub> at 2 eV) are observed in response to the photoexcitation of the perovskite matrix.<sup>17,18</sup> On the contrary, an apparently weaker emission of the pristine double perovskite compared to the un-doped sample (fair comparison has been done between absorption values and measurements to make the PL intensities among all the thin films comparable) at 2 eV is found, accompanied by a second, even weaker peak at 1.3 eV, which cannot be traced back to any typical Eu PL feature. The PL lifetime of the double perovskite is also considerably reduced (details in the S.I. Fig. S7). The weak PL signal at 1.3 eV could likely originate from deep defects within the band-gap of Cs<sub>2</sub>AgBiBr<sub>6</sub> as a consequence of Eu-doping and, therefore, could be seen as a sign of a trap-mediated recombination pathway.<sup>36</sup>

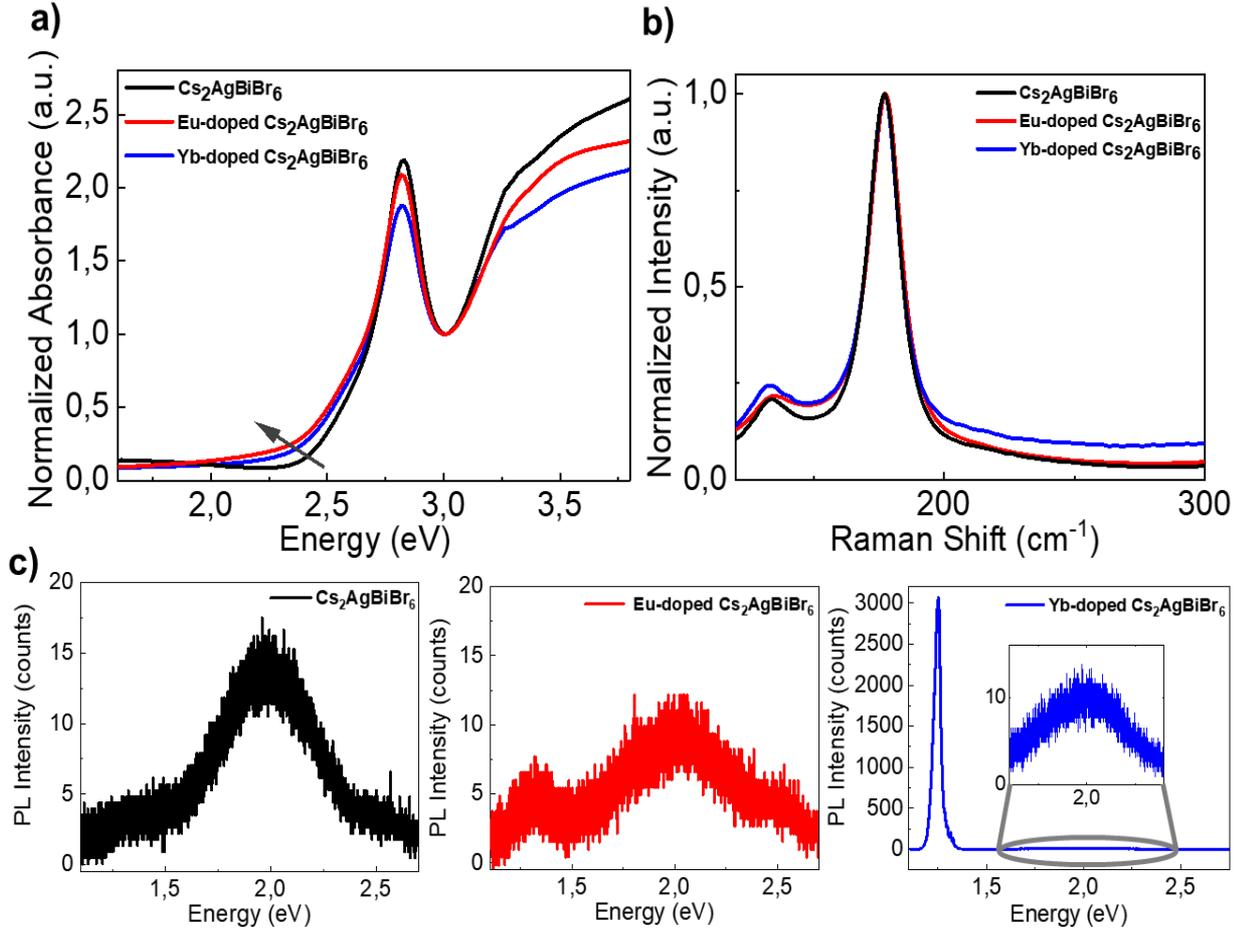


**Figure 2.** Optical properties of Eu- and Yb-doped Cs<sub>2</sub>AgBiBr<sub>6</sub>. a) Normalized (@ 3 eV) thin films absorption and b) Raman spectra of Eu- and Yb-doped Cs<sub>2</sub>AgBiBr<sub>6</sub> and of pristine Cs<sub>2</sub>AgBiBr<sub>6</sub> (532 nm laser excitation). c) Thin films steady-state photoluminescence (excitation @ 2.88 eV).

Doping with Yb(III) is expected to generate a sharp PL peak in the NIR at around 1.25 eV (1000 nm), as a result of the  ${}^2F_{5/2} \rightarrow {}^2F_{7/2}$  transition typical of this ion, as it has been seen before in analogous nanocrystal systems.<sup>20</sup> Such a peak is actually present and it is characterized by an extremely high intensity compared to the native PL of the double perovskite at 2 eV, as it can be observed from Fig. 2c (blue curve). The intensity ratio between these two PL contributions in the spectrum is in the order of 300:1. Notably, for the Yb-doped Cs<sub>2</sub>AgBiBr<sub>6</sub> nanocrystals described by Chen and coworkers<sup>20</sup> the native PL of the double perovskite was always significant even at the highest 5% doping concentration reported there and the maximum ratio achieved for the Yb-based peak relative to the double perovskite signal did not surpass the 2.5:1 ratio for the best case (at 2.9% Yb). Our data seem to indicate therefore that the Yb-dopant sensitization process (an energy transfer process from the photo-excited perovskite sensitizer to the lanthanide-based emissive centers) is much more efficient in the present thin films based on HT-synthesized bulk material than

in nanocrystals. Remarkably, a PL quantum yield (PLQY) of 28% ( $\pm 3\%$ ) is determined for Yb-doped  $\text{Cs}_2\text{AgBiBr}_6$  thin films, with net improvement from what found by Hoye et al.<sup>37</sup> for un-doped  $\text{Cs}_2\text{AgBiBr}_6$  thin films (0.02%). This is, to the best of our knowledge, the first report on the PLQY extent in Yb-doped  $\text{Cs}_2\text{AgBiBr}_6$  species, since for the case of nanocrystals previously discussed<sup>20</sup> this information was not provided.

We carried out a more detailed optical analysis of the NIR emission profile of Yb-doped  $\text{Cs}_2\text{AgBiBr}_6$  thin film by probing how the NIR-PL intensity varies as a function of the excitation wavelength. As it can be deduced from the excitation-PL 3D map reported in Fig. 3a and from the relative PLE spectrum in Fig. 3b (comparison with absorption is included for the sake of clarity), the maximum emission from the Yb(III) ions is achieved at an excitation energy of 2.58 eV and a second maximum of slightly minor intensity is also found at 3.02 eV. In between these two maxima is located a valley, with a minimum at around 2.8 eV, which is exactly the absorption energy corresponding to the exciton peak seen in the absorption profile. This behavior was reported previously by Zelewski et al.<sup>14</sup> for the pure  $\text{Cs}_2\text{AgBiBr}_6$  double perovskite single crystal and was interpreted as a further indication of the neutral character of the exciton-centered transition, that does not contribute to generate charges or to populate emissive trap states. It is therefore reasonable to believe that the present case provides further strength to this assumption, as also energy transfer processes between the exciton of the host semiconductor and the lanthanide dopants seem to be inefficient. A maximum of light emission is, instead, obtained when exciting in the low energy absorption edge (starting at 2.25 eV). As the relative absorption cross section at these energies is very low (dashed line), it indicates that i) the population of Yb states out of them occurs very efficiently and ii) the optical transition to these states must be strongly forbidden and they could be associated to those sub-band-gap states characteristic of the absorption profile. It is worthy to mention that such feature has been also found also by Zelewski et al. for the un-doped double perovskite.<sup>14</sup> The second plateau of the PLE spectrum (and of the excitation/NIR-PL 3D map), that resides in the 2.9-3.1 eV range, was indicated by some of us<sup>9</sup> as the absorption edge of a direct electronic transition in  $\text{Cs}_2\text{AgBiBr}_6$  occurring at 3.2 eV and extrapolated from the relative Tauc plot by applying the formula for direct band-gaps.

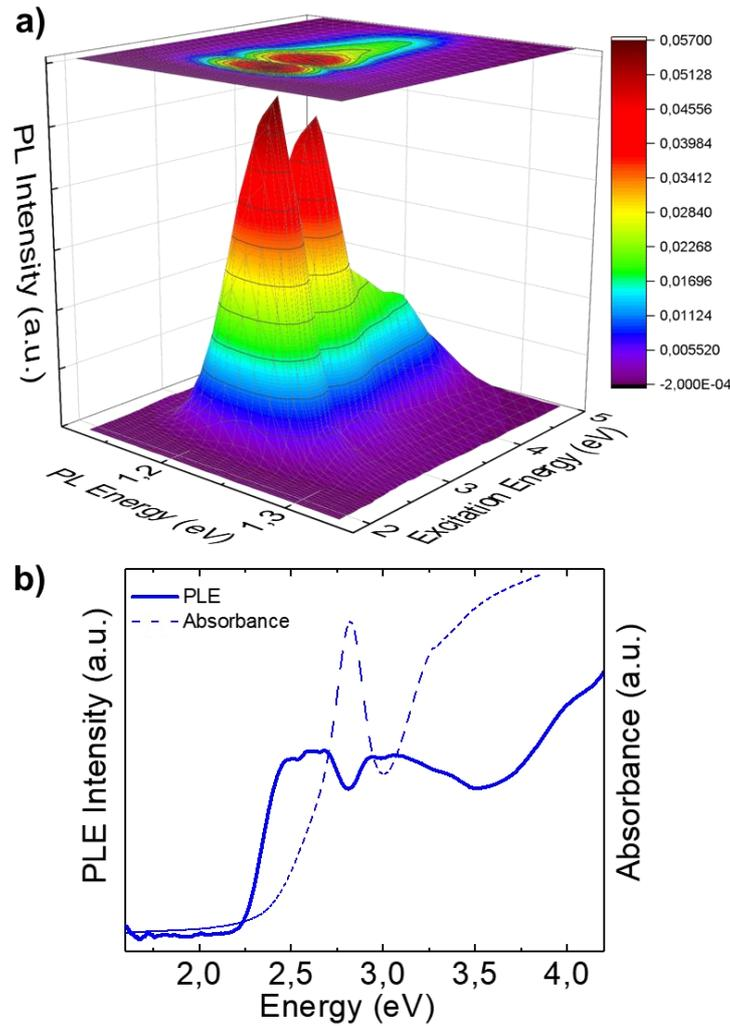


**Figure 3.** a) Excitation-NIR photoluminescence 3D map of an Yb-doped  $\text{Cs}_2\text{AgBiBr}_6$  thin film and b) corresponding photoluminescence excitation spectrum and comparison with absorption (dashed line).

The effects of Yb and Eu doping on the electronic properties of  $\text{Cs}_2\text{AgBiBr}_6$  have been investigated by density functional theory (DFT), by using the hybrid PBE0 functional (see Computational details in the S.I.).<sup>38,39</sup> Substitutional doping of Eu and Yb at the Bi site has been modelled by simulating dopant densities of  $\sim 3\%$ . In pristine  $\text{Cs}_2\text{AgBiBr}_6$   $\text{Bi}^{3+}$  ions are octahedrally coordinated by six  $\text{Br}^-$  at distance of 2.85 Å. Upon  $\text{Eu}^{3+}$  incorporation to form the  $\text{Eu}_{\text{Bi}}^0$  defect an asymmetric contraction of the lanthanide - bromide bond lengths in the octahedron unit is reported to values between 2.80-2.82 Å (Fig. 4b). The decreased bond length is ascribed to the smaller  $\text{Eu}^{3+}$  ionic radius of 109 pm compared to 117 pm for  $\text{Bi}^{3+}$ , as stated previously. A more pronounced contraction of the bond to  $\text{Br}^-$  to values of 2.72-2.75 Å was determined for Yb(III) incorporation, i.e. the  $\text{Yb}_{\text{Bi}}^0$  defect, showing a ionic radius even smaller than  $\text{Eu}^{3+}$ , i.e. 101 pm (Fig. 4e).

The projected density of states (PDOS) of the Eu and Yb doped  $\text{Cs}_2\text{AgBiBr}_6$  perovskite are reported in Fig. 4a and 4d.  $\text{Eu}_{\text{Bi}}^0$  and  $\text{Yb}_{\text{Bi}}^0$  show  $f^6$  and  $f^{13}$  electronic configurations and introduce unoccupied f-states into the band gap of  $\text{Cs}_2\text{AgBiBr}_6$ , placed at 1.70 eV and 1.59 eV above the valence band (VBM), respectively, with negligible impact on the band gap of the host perovskite (2.27 eV at the PBE0 level of theory). These single particle states are spatially localized on the dopants, as confirmed by the plot of the associated wavefunctions, reported in Fig. 4c and 4f. The emergence of unoccupied f-states within the band gap indicates that dopant sensitization may occur through vertical transitions of photo-excited electrons from the conduction band (CB) of the host perovskite to the mid-gap f-orbitals of the dopants.

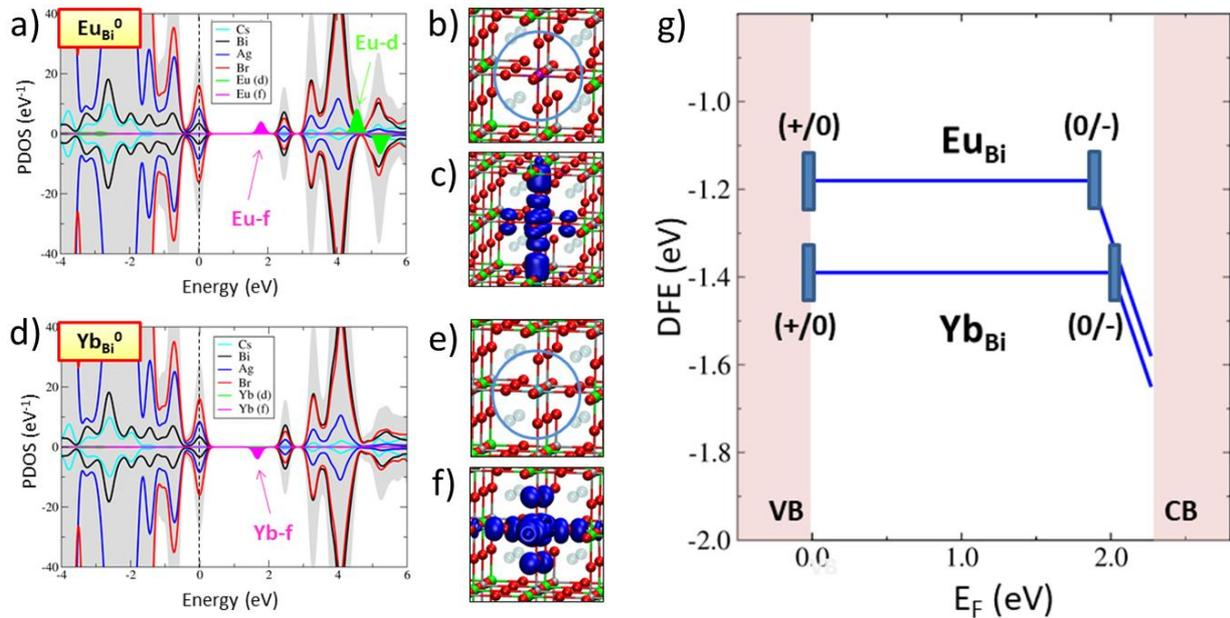


**Figure 4.** a) PDOS of Eu substituting Bi in the neutral state of charge, i.e.  $\text{Eu}_{\text{Bi}}^0$ , the top of VB has been set to zero of energy. b) optimized structure of  $\text{Eu}_{\text{Bi}}^0$  (Bi = green; Ag = grey; Br = red; Eu = purple; Yb = cyan); c) plot of the  $\text{Eu}_{\text{Bi}}^0$  LUMO single particle orbital associated to the unoccupied f state in the band gap of diagram 1a. d) PDOS of the  $\text{Yb}_{\text{Bi}}^0$  system. e) optimized structure and f) plot of the  $\text{Yb}_{\text{Bi}}^0$  LUMO single particle orbital; g) Defect formation energies and ionization levels of  $\text{Eu}_{\text{Bi}}$  and  $\text{Yb}_{\text{Bi}}$  defects in the  $\text{Cs}_2\text{BiAgBr}_6$  band gap, highlighting that electrons can be trapped through the deep (0/-) transitions, sensitizing the dopants.

The defect formation energies (DFE) and thermodynamic ionization levels (TIL) of  $\text{Eu}_{\text{Bi}}$  and  $\text{Yb}_{\text{Bi}}$  defects in different states of charge are reported in Figure 4g. DFEs have been estimated by considering metal exchange between the  $\text{EuCl}_3$ ,  $\text{YbCl}_3$  and  $\text{BiCl}_3$  molecules in the gas phase and the pristine perovskite. DFE diagram in Figure 4g shows that  $\text{Eu}_{\text{Bi}}$  and  $\text{Yb}_{\text{Bi}}$  defects are mainly stable in the neutral form (+III oxidation state) in the  $\text{Cs}_2\text{AgBiBr}_6$  band gap. Favourable substitutional energies of -1.18 and -1.39 eV for Eu and Yb were calculated, respectively, highlighting that the Yb-doping is slightly more favoured than Eu-doping.  $\text{Eu}_{\text{Bi}}$  and  $\text{Yb}_{\text{Bi}}$  show deep (0/-) transitions in the n-doped region of the diagrams placed at 1.87 and 2.01 eV above the VBM, respectively. This indicates that the +II oxidation state of the dopants is thermodynamically stable only in heavily n-doped perovskites. Upon electron trapping on the  $\text{Eu}_{\text{Bi}}^0$  and  $\text{Yb}_{\text{Bi}}^0$  centers to form  $\text{Eu}_{\text{Bi}}^-$  and  $\text{Yb}_{\text{Bi}}^-$  an increase of the Eu-Br and Yb-Br bond lengths to values of 2.92 Å and 2.80-2.84 Å is observed, respectively. In both cases a remarkable upshift in energy of the occupied f levels within the host perovskite band gap is reported (Fig. S8).

On the other hand, (+/0) transitions, associated to the introduction of one hole in the supercells, are only shallow, indicating that holes are delocalized in the VB of doped perovskite and cannot be trapped at Eu and Yb sites, which are stable only in the +III oxidation state in the Fermi level range delimited by the VBM and the (0/-) transition.

Defect analysis suggests that Eu- and Yb-dopants, once incorporated in substitutional position to Bi, can be activated upon photoexcitation through the electron trapping on the empty f-orbitals placed in the band gap. Relaxation of the excited dopant may occur through a recombination of the trapped electron with hole in the VB, or through a more complex mechanism involving the electron release and the conversion to form the neutral excited state of the dopant. In order to predict the possible trap assisted emission from the defects, *i.e.* the recombination of trapped electron with hole in the VB, the configuration diagrams of the ground and excited state of  $\text{Eu}_{\text{Bi}}$  and  $\text{Yb}_{\text{Bi}}$  have been calculated, they are reported in Figure S9 of S.I. Radiative emissions at 1.44 and 1.77 eV are calculated for Eu and Yb, respectively. The calculated emission at 1.44 eV for Eu-doped double perovskite is in close agreement with the weak PL peak at ~1.3 eV observed in optical experiments; thus, the origin of this PL feature may be ascribed to a trap mediated process involving the trapping of the electron with the subsequent recombination with hole in the VB. On the other hand, no sub-gap emissive transition at ~1.7 eV have been observed in the Yb-doped perovskite, suggesting that the activated  $\text{Yb}_{\text{Bi}}^-$  mainly rearrange to form the  $F_{5/2}$  neutral excited state by releasing the trapped electron to the CB and decaying with the characteristic emission at 1.25 eV observed in the PL (Fig. 2c, blue line). Such mechanism is partially justified by the higher optical (0/-) transition of  $\text{Yb}_{\text{Bi}}$  compared to  $\text{Eu}_{\text{Bi}}$ , exceeding the  $\text{Cs}_2\text{BiAgBr}_6$  band gap (see Fig. S9). Recombination of trapped

electrons with background holes, however, remains a competitive deactivation channel possibly reducing the PL efficiency of the f-f transition.

Based on experimental and theoretical evidence, a Jablonski diagram is proposed as the one reported in Fig. 5, depicting the process of lanthanide dopants activation after light excitation of the double perovskite. In this diagram it is shown, together with native and relatively weak PL of the un-doped double perovskite, also the very weak PL originated by the trapping of photoexcited electrons in the Eu-generated deep defects in the band gap and, oppositely, the more efficient energy transfer to the NIR-emissive  ${}^2F_{5/2} \rightarrow {}^2F_{7/2}$  transition of the  $\text{Yb}^{3+}$  ions.

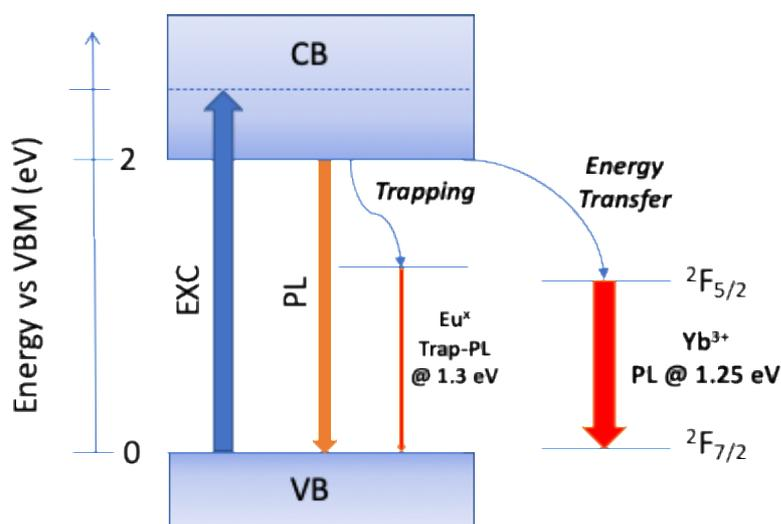


**Figure 5.** Jablonski diagram depicting the excited state deactivation processes happening in undoped, Eu- and Yb-doped  $\text{Cs}_2\text{AgBiBr}_6$ . Here CBM is taken at an energy corresponding to the PL maximum of the  $\text{Cs}_2\text{AgBiBr}_6$  thin film, while the excitation (thick blue line) is indicated to take place at a general energy (dashed line in the CB) which is higher than the energy of the CBM, given the pronounced Stokes' shift existing between absorption and emission profiles in the un-doped double perovskite. The thickness of the three PL lines (orange to red) is proportional to the relative intensity of the indicated transitions.

In conclusion, we have shown that Yb(III) doping in thin films of the lead-free  $\text{Cs}_2\text{AgBiBr}_6$  double perovskite that are processed from the bulk HT powder material can lead to the detection of a narrow and unique PL signal located in the NIR. This points out at an efficient energy transfer from the photoexcited double perovskite host to the rare earth guest that was not observed before in similar nanocrystal systems. We have also provided theoretical insights on the lanthanide-sensitization process, which will be extremely useful for designing future doping strategies in lead-

free double perovskites. We believe that the bulk Yb-doped Cs<sub>2</sub>AgBiBr<sub>6</sub> thin films described in this work hold great promises for the future realization of NIR-emissive solid-state devices after further optimization of the doping level and overall layer quality,<sup>7</sup> as they are easy-to-process and feature a unique and well-defined emission profile.

## Acknowledgements

F.S., J.H., D.S. and T.G. acknowledge the DFG for financial support *via* the GRK (Research Training Group) 2204 "Substitute Materials for Sustainable Energy Technologies". K.G. acknowledges funding from the Royal Society through a Newton International Fellowship. F.L. thanks the Centre Giorgio Levi Cases for Energy Economics and Technology of the University of Padova for the project "AMON-RA". F.C. acknowledges the Royal Society for the award of a Wolfson Foundation Research Merit Award. We thank Prof. Lorenzo Franco for insightful discussion.

## Supporting Information

Experimental and computational details; results from analytical and structural characterization (elemental analysis, XRD, TEM, SEM); KPFM data; time-resolved photoluminescence data; additional details from DFT calculations

## References

- (1) Wang, R.; Wang, J.; Tan, S.; Duan, Y.; Wang, Z.-K.; Yang, Y. Opportunities and Challenges of Lead-Free Perovskite Optoelectronic Devices. *Trends Chem.* **2019**, *1* (4), 368–379.
- (2) Wang, X.; Zhang, T.; Lou, Y.; Zhao, Y. All-Inorganic Lead-Free Perovskites for Optoelectronic Applications. *Mater. Chem. Front.* **2019**, *3* (3), 365–375.
- (3) Yu, B.-B.; Liao, M.; Zhu, Y.; Zhang, X.; Du, Z.; Jin, Z.; Liu, D.; Wang, Y.; Gatti, T.; Ageev, O.; He, Z. Oriented Crystallization of Mixed-Cation Tin Halides for Highly Efficient and Stable Lead-Free Perovskite Solar Cells. *Adv. Funct. Mater.* **2020**, *30* (24), 2002230.
- (4) Ke, W.; Kanatzidis, M. G. Prospects for Low-Toxicity Lead-Free Perovskite Solar Cells. *Nat. Commun.* **2019**, *10* (1), 965.
- (5) Li, J.; Cao, H.-L.; Jiao, W.-B.; Wang, Q.; Wei, M.; Cantone, I.; Lü, J.; Abate, A. Biological Impact of Lead from Halide Perovskites Reveals the Risk of Introducing a Safe Threshold. *Nat. Commun.* **2020**, *11* (1), 310.
- (6) Zhang, L.; Wang, K.; Zou, B. Bismuth Halide Perovskite-Like Materials: Current Opportunities and Challenges. *ChemSusChem* **2019**, *12* (8), 1612–1630.

- (7) Jin, Z.; Zhang, Z.; Xiu, J.; Song, H.; Gatti, T.; He, Z. A Critical Review on Bismuth and Antimony Halides Based Perovskites and Derivatives for Photovoltaic Applications: Recent Advances and Challenges. *J. Mater. Chem. A* **2020**, *8* (32), 16166–16188.
- (8) Liu, D.; Yu, B.-B.; Liao, M.; Jin, Z.; Zhou, L.; Zhang, X.; Wang, F.; He, H.; Gatti, T.; He, Z. Self-Powered and Broadband Lead-Free Inorganic Perovskite Photodetector with High Stability. *ACS Appl. Mater. Interfaces* **2020**, *12* (27), 30530–30537.
- (9) Kentsch, R.; Scholz, M.; Horn, J.; Schlettwein, D.; Oum, K.; Lenzer, T. Exciton Dynamics and Electron–Phonon Coupling Affect the Photovoltaic Performance of the Cs<sub>2</sub>AgBiBr<sub>6</sub> Double Perovskite. *J. Phys. Chem. C* **2018**, *122* (45), 25940–25947.
- (10) Xiu, J.; Shao, Y.; Chen, L.; Feng, Y.; Dai, J.; Zhang, X.; Lin, Y.; Zhu, Y.; Wu, Z.; Zheng, Y.; Pan, H.; Liu, C.; Shi, X.; Cheng, X.; He, Z. Defining the Composition and Electronic Structure of Large-Scale and Single-Crystalline like Cs<sub>2</sub>AgBiBr<sub>6</sub> Films Fabricated by Capillary-Assisted Dip-Coating Method. *Mater. Today Energy* **2019**, *12*, 186–197.
- (11) Wu, C.; Zhang, Q.; Liu, Y.; Luo, W.; Guo, X.; Huang, Z.; Ting, H.; Sun, W.; Zhong, X.; Wei, S.; Wang, S.; Chen, Z.; Xiao, L. The Dawn of Lead-Free Perovskite Solar Cell: Highly Stable Double Perovskite Cs<sub>2</sub>AgBiBr<sub>6</sub> Film. *Adv. Sci.* **2018**, *5* (3), 1700759.
- (12) Gao, W.; Ran, C.; Xi, J.; Jiao, B.; Zhang, W.; Wu, M.; Hou, X.; Wu, Z. High-Quality Cs<sub>2</sub>AgBiBr<sub>6</sub> Double Perovskite Film for Lead-Free Inverted Planar Heterojunction Solar Cells with 2.2 % Efficiency. *ChemPhysChem* **2018**, *19* (14), 1696–1700.
- (13) Igbari, F.; Wang, R.; Wang, Z.-K.; Ma, X.-J.; Wang, Q.; Wang, K.-L.; Zhang, Y.; Liao, L.-S.; Yang, Y. Composition Stoichiometry of Cs<sub>2</sub>AgBiBr<sub>6</sub> Films for Highly Efficient Lead-Free Perovskite Solar Cells. *Nano Lett.* **2019**, *19* (3), 2066–2073.
- (14) Zelewski, S. J.; Urban, J. M.; Surrente, A.; Maude, D. K.; Kuc, A.; Schade, L.; Johnson, R. D.; Dollmann, M.; Nayak, P. K.; Snaith, H. J.; Radaelli, P.; Kudrawiec, R.; Nicholas, R. J.; Plochocka, P.; Baranowski, M. Revealing the Nature of Photoluminescence Emission in the Metal-Halide Double Perovskite Cs<sub>2</sub>AgBiBr<sub>6</sub>. *J. Mater. Chem. C* **2019**, *7* (27), 8350–8356.
- (15) Kumar, V.; Ntwaeaborwa, O. M.; Soga, T.; Dutta, V.; Swart, H. C. Rare Earth Doped Zinc Oxide Nanophosphor Powder: A Future Material for Solid State Lighting and Solar Cells. *ACS Photonics* **2017**, *4* (11), 2613–2637.
- (16) Heine, J.; Müller-Buschbaum, K. Engineering Metal-Based Luminescence in Coordination Polymers and Metal–Organic Frameworks. *Chem. Soc. Rev.* **2013**, *42* (24), 9232–9242.
- (17) Mir, W. J.; Sheikh, T.; Arfin, H.; Xia, Z.; Nag, A. Lanthanide Doping in Metal Halide Perovskite Nanocrystals: Spectral Shifting, Quantum Cutting and Optoelectronic Applications. *NPG Asia Mater.* **2020**, *12* (1), 9.

- (18) Righetto, M.; Meggiolaro, D.; Rizzo, A.; Sorrentino, R.; He, Z.; Meneghesso, G.; Sum, T. C.; Gatti, T.; Lamberti, F. Coupling Halide Perovskites with Different Materials: From Doping to Nanocomposites, beyond Photovoltaics. *Prog. Mater. Sci.* **2020**, *110*, 100639.
- (19) Milstein, T. J.; Kroupa, D. M.; Gamelin, D. R. Picosecond Quantum Cutting Generates Photoluminescence Quantum Yields Over 100% in Ytterbium-Doped CsPbCl<sub>3</sub> Nanocrystals. *Nano Lett.* **2018**, *18* (6), 3792–3799.
- (20) Chen, N.; Cai, T.; Li, W.; Hills-Kimball, K.; Yang, H.; Que, M.; Nagaoka, Y.; Liu, Z.; Yang, D.; Dong, A.; Xu, C.-Y.; Zia, R.; Chen, O. Yb- and Mn-Doped Lead-Free Double Perovskite Cs<sub>2</sub>AgBiX<sub>6</sub> (X = Cl<sup>-</sup>, Br<sup>-</sup>) Nanocrystals. *ACS Appl. Mater. Interfaces* **2019**, *11* (18), 16855–16863.
- (21) Kimura, T.; Yokoi, A.; Nishida, Y.; Saito, R.; Yugo, S.; Ikoma, T. Photoluminescence of Ytterbium-doped Porous Silicon. *Appl. Phys. Lett.* **1995**, *67* (18), 2687–2689.
- (22) Iyer, S. S.; Xie, Y.-H. Light Emission from Silicon. *Science* **1993**, *260* (5104), 40–46.
- (23) Adjokatse, S.; Fang, H.-H.; Loi, M. A. Broadly Tunable Metal Halide Perovskites for Solid-State Light-Emission Applications. *Mater. Today* **2017**, *20* (8), 413–424.
- (24) Yan, F.; Demir, H. V. LEDs Using Halide Perovskite Nanocrystal Emitters. *Nanoscale* **2019**, *11* (24), 11402–11412.
- (25) Yan, F.; Tan, S. T.; Li, X.; Demir, H. V. Light Generation in Lead Halide Perovskite Nanocrystals: LEDs, Color Converters, Lasers, and Other Applications. *Small* **2019**, *15* (47), 1902079.
- (26) Lamberti, F.; Litti, L.; De Bastiani, M.; Sorrentino, R.; Gandini, M.; Meneghetti, M.; Petrozza, A. High-Quality, Ligands-Free, Mixed-Halide Perovskite Nanocrystals Inks for Optoelectronic Applications. *Adv. Energy Mater.* **2017**, *7* (8), 1601703.
- (27) Greul, E.; Petrus, M. L.; Binek, A.; Docampo, P.; Bein, T. Highly Stable, Phase Pure Cs<sub>2</sub>AgBiBr<sub>6</sub> Double Perovskite Thin Films for Optoelectronic Applications. *J. Mater. Chem. A* **2017**, *5* (37), 19972–19981.
- (28) Jeon, N. J.; Noh, J. H.; Kim, Y. C.; Yang, W. S.; Ryu, S.; Seok, S. Il. Solvent Engineering for High-Performance Inorganic–Organic Hybrid Perovskite Solar Cells. *Nat. Mater.* **2014**, *13* (9), 897–903.
- (29) Pantaler, M.; Cho, K. T.; Queloz, V. I. E.; García Benito, I.; Fettkenhauer, C.; Anusca, I.; Nazeeruddin, M. K.; Lupascu, D. C.; Grancini, G. Hysteresis-Free Lead-Free Double-Perovskite Solar Cells by Interface Engineering. *ACS Energy Lett.* **2018**, *3* (8), 1781–1786.
- (30) McClure, E. T.; Ball, M. R.; Windl, W.; Woodward, P. M. Cs<sub>2</sub>AgBiX<sub>6</sub> (X = Br, Cl): New Visible Light Absorbing, Lead-Free Halide Perovskite Semiconductors. *Chem. Mater.* **2016**,

28 (5), 1348–1354.

- (31) Ono, L. K.; Liu, S. (Frank); Qi, Y. Reducing Detrimental Defects for High-Performance Metal Halide Perovskite Solar Cells. *Angew. Chemie Int. Ed.* **2020**, *59* (17), 6676–6698.
- (32) Bekenstein, Y.; Dahl, J. C.; Huang, J.; Osowiecki, W. T.; Swabeck, J. K.; Chan, E. M.; Yang, P.; Alivisatos, A. P. The Making and Breaking of Lead-Free Double Perovskite Nanocrystals of Cesium Silver–Bismuth Halide Compositions. *Nano Lett.* **2018**, *18* (6), 3502–3508.
- (33) Dey, A.; Richter, A. F.; Debnath, T.; Huang, H.; Polavarapu, L.; Feldmann, J. Transfer of Direct to Indirect Bound Excitons by Electron Intervalley Scattering in Cs<sub>2</sub>AgBiBr<sub>6</sub> Double Perovskite Nanocrystals. *ACS Nano* **2020**, *14* (5), 5855–5861.
- (34) Longo, G.; Mahesh, S.; Buizza, L. R. V; Wright, A. D.; Ramadan, A. J.; Abdi-Jalebi, M.; Nayak, P. K.; Herz, L. M.; Snaith, H. J. Understanding the Performance Limiting Factors of Cs<sub>2</sub>AgBiBr<sub>6</sub> Double-Perovskite Solar Cells. *ACS Energy Lett.* **2020**.
- (35) Slavney, A. H.; Hu, T.; Lindenberg, A. M.; Karunadasa, H. I. A Bismuth-Halide Double Perovskite with Long Carrier Recombination Lifetime for Photovoltaic Applications. *J. Am. Chem. Soc.* **2016**, *138* (7), 2138–2141.
- (36) Motti, S. G.; Gandini, M.; Barker, A. J.; Ball, J. M.; Srimath Kandada, A. R.; Petrozza, A. Photoinduced Emissive Trap States in Lead Halide Perovskite Semiconductors. *ACS Energy Lett.* **2016**, *1*, 726–730.
- (37) Hoye, R. L. Z.; Eyre, L.; Wei, F.; Brivio, F.; Sadhanala, A.; Sun, S.; Li, W.; Zhang, K. H. L.; MacManus-Driscoll, J. L.; Bristowe, P. D.; Friend, R. H.; Cheetham, A. K.; Deschler, F. Fundamental Carrier Lifetime Exceeding 1 Ms in Cs<sub>2</sub>AgBiBr<sub>6</sub> Double Perovskite. *Adv. Mater. Interfaces* **2018**, *5* (15), 1800464.
- (38) Adamo, C.; Barone, V. Toward Reliable Density Functional Methods without Adjustable Parameters: The PBE0 Model. *J. Chem. Phys.* **1999**, *110* (13), 6158–6170.
- (39) Perdew, J. P.; Ernzerhof, M.; Burke, K. Rationale for Mixing Exact Exchange with Density Functional Approximations. *J. Chem. Phys.* **1996**, *105*, 9982–9985.